JCTC Journal of Chemical Theory and Computation

Article

pubs.acs.org/JCTC

Low Scaling Algorithms for the Random Phase Approximation: Imaginary Time and Laplace Transformations

Merzuk Kaltak,* Jiří Klimeš, and Georg Kresse

University of Vienna, Faculty of Physics and Center for Computational Materials Science, Sensengasse 8/12, A-1090 Vienna, Austria

ABSTRACT: In this paper, we determine efficient imaginary frequency and imaginary time grids for second-order Møller−Plesset (MP) perturbation theory. The least-squares and Minimax quadratures are compared for periodic systems, finding that the Minimax quadrature performs slightly better for the considered materials. We show that the imaginary frequency grids developed for second order also perform well for the correlation energy in the direct random phase approximation. Furthermore, we show that the polarizabilities on the imaginary time axis can be Fourier-transformed to the imaginary frequency domain, since the time and frequency Minimax grids are dual to each other. The same duality is observed for the least-squares grids. The transformation from imaginary time to imaginary frequency allows one to reduce the time complexity to cubic (in system size), so that random phase approximation (RPA) correlation energies become accessible for large systems.

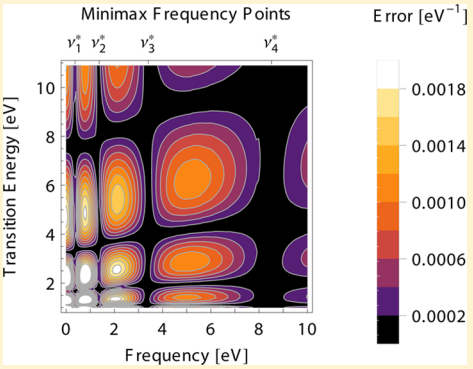

1. INTRODUCTION

Energy denominators of the form $1/x$, with x denoting transition energies between occupied and unoccupied states, appear naturally in Møller−Plesset perturbation theory (MPPT).[1] Almlöf replaced the energy denominators by an integral using the identity

$$\frac{1}{x} = \int_0^\infty \mathrm{d}\tau\ \mathrm{e}^{-x\tau} \qquad x > 0 \tag{1}$$

and evaluated the right-hand side (r.h.s.) of eq 1 by means of a quadrature formula.[2] Nowadays, this approach is known as the Laplace-transformed Møller−Plesset (LT-MP) technique and has the favorable property that the computational effort of second-order Møller−Plesset (MP2) calculations scales with the fourth power of the system size M.[3] Because of the latter, the LT-MP method has gained some attention in the quantum chemistry community in the past 20 years.[3−6]

Since numerical quadrature rules for the integral on the r.h.s. of eq 1 play an important role in LT-MP2, several studies have sought to construct optimal rules.[6,7] The quadrature rules for the Laplace integral in eq 1 are typically obtained from a least-squares fit of the $1/x$ function.[3] In a recent paper, however, Takatsuka et al. proposed to apply the Minimax approximation.[8] This approximation is referred to as the "best approximation", in the sense that it minimizes the maximum error of the quadrature.[9] Apart from the latter the Minimax approximation distributes the error uniformly along the entire range of transition energies x, so that an effective error cancellation is more likely than for any other quadrature.[10]

Application of Laplace transformations to methods beyond the MP2 energies are fairly rare. One important approximation for the correlation energy is the random phase approximation (RPA).[11−16] The RPA is an infinite sum of bubble diagrams, corresponding to the direct terms in MP perturbation theory.[17] In the past 10 years, RPA has been applied successfully to various phenomena in condensed-matter physics, such as the adsorption of CO on metallic surfaces, the description of van der Waals interactions, or bulk properties of transition metals.[18−21]

The computational cost for conventional RPA calculations for periodic systems grows with the fourth power of M.[21−25] The bottleneck hereby is the direct evaluation of the polarizability χ, using the Adler and Wiser formula, limiting the application of RPA to $O(100)$ electrons.[26−28]

In principle, one is able to evaluate χ with $O(M^3)$ scaling using the imaginary time Green's functions $G(\mathbf{r},\mathbf{r}',i\tau)$ and Hedin's equation for the independent particle polarizability,[29]

$$\hat{\chi}(\mathbf{r}, \mathbf{r}', i\tau) = -G(\mathbf{r}, \mathbf{r}', i\tau)G(\mathbf{r}', \mathbf{r}, -i\tau) \tag{2}$$

This approach was discussed by Rojas et al.[30] and was recently implemented for molecules by Foerster et al.[31] A different approach, allowing for the inclusion of second-order exchange corrections, was presented for molecules by Moussa,[32] but a cubic-scaling RPA algorithm for periodic systems has not been implemented.

The reasons are mainly technical. Equation 2 gives the polarizability in the imaginary time domain, so that one needs to Fourier transform $\hat{\chi}(i\tau)$ to the imaginary frequency domain $\chi(i\nu)$ in order to evaluate the RPA energy. For an accurate discrete Fourier transformation, an equally spaced grid for the time and frequency domain necessitates a few hundred grid points.[33] This makes the calculations rather expensive, so that the break-even point between the traditional $O(M^4)$ algorithm and the lower scaling $O(M^3)$ algorithm is reached only for very large systems. Such large systems are then also difficult to

Received: February 13, 2014
Published: April 23, 2014

   dx.doi.org/10.1021/ct5001268 | J. Chem. Theory Comput. 2014, 10, 2498−2507

handle, since the storage demands for the polarizability at many frequency points can easily exceed the available memory, even on modern large-scale computers. This implies that the approach can be applied to large systems only if the number of grid points τ_i, ν_b, which are needed for an accurate representation and Fourier transformation of $\chi(i\tau)$ and $\chi(i\nu)$, is kept as small as possible.

In this work, we first determine tailor-made quadratures for the direct MP2 energy in the *imaginary frequency* domain (as opposed to the usual imaginary time domain used in LT-MP2). Apart from comparing the Minimax and least-squares quadratures for the LT-MP2 method, we show that our frequency grid is also able to integrate the RPA correlation energy accurately using ∼10−20 quadrature points. In addition, approximating the Fourier integral of the polarizability by means of a quadrature formula, we find an elegant method to switch from imaginary time to imaginary frequency polarizabilities and vice versa without using an interpolation technique or significantly increasing the number of quadrature points. This allows to evaluate RPA energies with well-controlled approximations (time and frequency grids) with $O(M^3)$ scaling.

The paper is organized as follows. In sections 2.1 and 2.2, we review the necessary mathematical background for tailor-made quadrature formulas. In section 2.3, we present a method for the accurate determination of the cosine integral of χ, in terms of the imaginary time counterpart $\hat{\chi}$. We discuss its application to an RPA algorithm, which scales cubically with the considered system size. In section 3, we compare the convergence behavior of the Minimax and least-squares quadratures for MP2 and RPA calculations. In addition, results for RPA and direct MP2 energies using the nonuniform cosine transformation established in section 2.3 are given in section 3.

2. THEORY

2.1. The Fitting Problem. Given a function f: $I = [1,R] \to \mathbb{R}$ with $R > 1$ and a model function φ: $\mathbb{R} \times I \to \mathbb{R}$, the fitting problem is stated as follows: find the set of coefficients $\vec{\alpha} = (\alpha_1, ..., \alpha_N)$, $\vec{\beta} = (\beta_1, ..., \beta_N) \in \mathbb{R}^N$ such that the error function

$$\eta(\vec{\alpha}, \vec{\beta}, x) = f(x) - \sum_{i=1}^{N} \beta_i \varphi(\alpha_i, x) \tag{3}$$

is minimal, with respect to one of the following norms:

$$\| \eta \|_2 = \int_1^R \mathrm{d}x \, |\eta(\vec{\alpha}, \vec{\beta}, x)|^2 \tag{4}$$

$$\| \eta \|_\infty = \max\{|\eta(\vec{\alpha}, \vec{\beta}, x)| \in \mathbb{R} : x \in I\} \tag{5}$$

Minimization with respect to $\|\cdot\|_2$ gives the least-squares coefficients $\vec{\alpha}^0$ and $\vec{\beta}^0$. The corresponding fit minimizes the average or *mean error*, but results in an uneven distribution of the error in the interval I, with errors maximal toward $x \to 1$ (for the functions f considered here). A possible way of computing $\vec{\alpha}^0$ and $\vec{\beta}^0$ for nonlinear fitting problems is the Levenberg−Marquardt algorithm.[34]

On the other side, minimizing η with respect to $\|\cdot\|_\infty$ gives the so-called Minimax solution $\vec{\alpha}^*, \vec{\beta}^*$.[9] This means that the *maximum error* is minimized and the error is consequently equally distributed inside the interval I. Usually, this is desired, because contributions from small x are most important and dominate the final error. Note that, throughout this paper, we will always use an asterisk, α_i^*, β_i^*, when referring to grids and weights corresponding to Minimax solutions, whereas the conventional least-squares grids will carry the superscript 0.

Implementations calculating $\vec{\alpha}^*, \vec{\beta}^*$ typically use the Remez algorithm, which relies on Chebyshev's alternation theorem.[35] This theorem states that, in the Minimax approximation, the error function satisfies

$$\eta(\vec{\alpha}^*, \vec{\beta}^*, x_j) = (-1)^j \varepsilon \qquad \forall\, j = 1, ..., 2N + 1 \tag{6}$$

where the points x_j are the local extrema of η. In total, there are $2N + 1$ minima and maxima, leading to $2N + 1$ linear independent equations (eq 6: $2N$ equations for the coefficients $\vec{\alpha}, \vec{\beta}$ and one for the minimized error extremum ε.

Assuming we have a starting guess (say $\vec{\alpha}^0$ and $\vec{\beta}^0$ for the coefficients, we can apply the Remez algorithm:

(i) Find all extrema $\{x_j\}_{j=1}^{2N+1}$ of η.
(ii) Solve eq 6 for $\vec{\alpha}$, $\vec{\beta}$, and ε at the determined extrema x_j.
(iii) Update coefficients and error $\vec{\alpha}$, $\vec{\beta}$, and ε.
(iv) Iterate steps (i)−(iii) until convergence.

The solution of the fitting problem can be used in order to determine optimal quadrature formulas for the numerical evaluation of integrals. In the following, we discuss the application for a certain set of integrals.

2.2. Integral Quadrature Formulas for RPA and Direct MP Energies. We are interested primarily in the numerical evaluation of the RPA correlation energy:[13,36]

$$E_c^{\mathrm{RPA}} = \frac{1}{2\pi} \int_0^\infty \mathrm{d}\nu \; \mathrm{Tr}\{\ln(1 - \chi(i\nu)V) + \chi(i\nu)V\}$$
$$\text{with } \chi(i\nu) = \chi(-i\nu) \tag{7}$$

Here, χ is the independent particle polarizability on the imaginary frequency axis $\omega = i\nu$ and V is the Coulomb potential. In the following, we suppress the trace symbol.

The series expansion of $\ln(1 - x) = -\sum_{i=1}^{\infty} (x^n/n)$ in eq 7 implies a series expansion for the correlation energy $E_c = E_c^{(2)} + E_c^{(3)} + \cdots$, where

$$E_c^{(n)} = -\frac{1}{4\pi} \frac{1}{n} \int_{-\infty}^{\infty} \mathrm{d}\nu \; \{\chi(i\nu)V\}^n \qquad n \geq 2 \tag{8}$$

$E_c^{(n)}$ are the direct MP correlation energies for order n.[17,23] The lowest contribution, $n = 2$, the direct MP2 correlation energy, reads as follows:[17,23]

$$E_c^{(2)} = -\frac{1}{8\pi} \int_{-\infty}^{\infty} \mathrm{d}\nu \; \{\chi(i\nu)V\}^2 \tag{9}$$

Instead of evaluating this integral in the *imaginary frequency* domain, we can insert the Fourier transformation

$$\chi(i\nu) = \int_{-\infty}^{\infty} \mathrm{d}\tau \; \hat{\chi}(i\tau) \, \mathrm{e}^{i\nu\tau} \tag{10}$$

into eq 9 and use $\int \mathrm{d}\nu \; \mathrm{e}^{i\nu(\tau+\tau')} = 2\pi\delta(\tau + \tau')$ in order to obtain the corresponding *imaginary time* representation,

$$E_c^{(2)} = -\frac{1}{4} \int_{-\infty}^{\infty} \mathrm{d}\tau \; \{\hat{\chi}(i\tau)V\}^2 \tag{11}$$

This expression is the Laplace-transformed direct MP2 energy used by Häser and Almlöf.[3]

In obtaining eq 11, we used the fact that both representations of the polarizability χ and $\hat{\chi}$ are even functions in their arguments ν and τ, respectively. We note that the symmetry $\chi(i\nu) = \chi(-i\nu)$ implies the same for the time domain

dx.doi.org/10.1021/ct5001268 | J. Chem. Theory Comput. 2014, 10, 2498−2507

$\hat{\chi}(i\tau) = \hat{\chi}(-i\tau)$, so that, consequently, the Fourier transformation becomes a cosine transformation

$$\chi(i\nu) = 2\int_0^\infty \mathrm{d}\tau\, \hat{\chi}(i\tau)\cos(\tau\nu) \tag{12}$$

$$\hat{\chi}(i\tau) = \frac{1}{\pi}\int_0^\infty \mathrm{d}\nu\, \chi(i\nu)\cos(\tau\nu) \tag{13}$$

For the evaluation of the integrals described by eqs 9 and 11, only the frequency and time dependence of the polarizability is relevant. Fortunately, both the frequency and time dependence are well-known and were studied independently by Adler and Wiser in the 1960s.[26,27] The explicit form of the independent particle polarizability reads[28,37]

$$\chi(i\nu) = \sum_\mu \chi_\mu \phi(\nu, x_\mu) \tag{14}$$

$$\hat{\chi}(i\tau) = \sum_\mu \chi_\mu \hat{\phi}(\tau, x_\mu) \tag{15}$$

where we introduced the auxiliary functions

$$\phi(\nu, x) := \frac{2x}{x^2 + \nu^2} \tag{16}$$

$$\hat{\phi}(\tau, x) := \mathrm{e}^{-x|\tau|} \tag{17}$$

describing the frequency and the time dependence, respectively, and we have adopted the following notation in eqs 14 and 15:

- μ stands for the compound index (i,a), where i goes over occupied states and a goes over unoccupied states,
- x_μ is the transition energy between unoccupied states a and occupied states i ($x_\mu = \varepsilon_a - \varepsilon_i > 0$), and
- χ_μ represents a matrix χ_μ with dimensions given by the number of reciprocal lattice vectors $|\mathbf{G}|^2\hbar/(2m) \le E_{\mathrm{cut}}$ ($\chi_\mu = \langle i|\mathrm{e}^{i\mathbf{G}\mathbf{r}}|a\rangle\langle a|\mathrm{e}^{-i\mathbf{G}'\mathbf{r}'}|i\rangle$). We note that other basis sets for the response function can be chosen as well (for instance, auxiliary Gaussian basis sets such as those used in refs 38 and 24).

We remind the reader that $\varepsilon_{\min} \le x_\mu \le \varepsilon_{\max}$, with $\varepsilon_{\min}$ being the band gap and $\varepsilon_{\max}$ the maximally considered transition energy.

Inserting either eq 15 into eq 11, or eq 14 into eq 9, the resulting integrals can be carried out analytically yielding an exact expression for the second-order direct Møller−Plesset energy (MP2) $E_c^{(2)}$ that is often used by quantum chemists:[1,3,17]

$$E_c^{(2)} = -\frac{1}{4}\sum_{\mu\mu'} \chi_\mu V \chi_{\mu'} V \frac{1}{x_\mu + x_{\mu'}} \tag{18}$$

Although this expression avoids a frequency respectively time integration, the scaling is not favorable, because it involves a summation over quadruples $(\mu,\mu') = (i,a,i',a')$.

If one evaluates the integrals given in eqs 9 and 11 numerically, by using an appropriate quadrature,

$$E_c^{(2)} \approx -\frac{1}{8\pi}\sum_{k=1}^N \gamma_k \{\chi(i\nu_k)V\}^2 \tag{19}$$

$$E_c^{(2)} \approx -\frac{1}{4}\sum_{i=1}^N \sigma_i \{\hat{\chi}(i\tau_i)V\}^2 \tag{20}$$

one can avoid the computationally expensive summation over pairs (μ,μ'). In order to keep the necessary quadrature points N as small as possible, the error stemming from the discretization of the frequency and time domain, respectively, needs to be investigated. For this purpose, we subtract eq 18 from eq 19 and substitute $\chi(i\nu)$ by eq 14, obtaining

$$\frac{1}{4}\sum_{\mu\mu'} \chi_\mu V \chi_{\mu'} V \left\{ \frac{1}{x_\mu + x_{\mu'}} - \frac{1}{2\pi}\sum_{k=1}^N \gamma_k \phi(\nu_k, x_\mu)\phi(\nu_k, x_{\mu'}) \right\} \tag{21}$$

The terms in the curly braces can be considered to be the error made when approximating the integral described by eq 9 by a discrete sum (eq 19). This means the error for each pair $(x,x') \in [\varepsilon_{\min},\varepsilon_{\max}] \times [\varepsilon_{\min},\varepsilon_{\max}]$ (where (x,x') are representatives of a pair $(x_\mu,x_{\mu'})$) is described by the function

$$\mathcal{H}(\vec{\gamma}, \vec{\nu}, x, x') = \frac{1}{x + x'} - \frac{1}{2\pi}\sum_{k=1}^N \gamma_k \phi(\nu_k, x)\phi(\nu_k, x') \tag{22}$$

Analogously, subtracting eq 18 from eq 20, one can define an error function $\hat{\mathcal{H}}$ for the time domain, which reads

$$\hat{\mathcal{H}}(\vec{\sigma}, \vec{\tau}, x+x') = \frac{1}{x+x'} - \sum_{i=1}^N \sigma_i \underbrace{\hat{\phi}(\tau_i, x)\hat{\phi}(\tau_i, x')}_{\mathrm{e}^{-(x+x')\tau_i}}. \tag{23}$$

The quadrature $(\vec{\gamma},\vec{\nu})$ $(\vec{\sigma},\vec{\tau})$, respectively) is accurate, if the error $\mathcal{H}$ ($\hat{\mathcal{H}}$, respectively) for each pair $(x,x') \in [\varepsilon_{\min},\varepsilon_{\max}] \times [\varepsilon_{\min},\varepsilon_{\max}]$ is small. For eq 23, the error function depends on $x + x'$ and is, consequently, one-dimensional. Therefore, one can find the desired quadrature $(\vec{\sigma},\vec{\tau})$ by solving the corresponding fitting problem for $f(x + x') = (x + x')^{-1}$ (compare section 2.1).[39]

However, the error function in the frequency domain defined in eq 22 depends on two linearly independent variables, x and x', so that a two-dimensional fitting problem needs to be solved. The corresponding least-squares solution (i.e., minimum of $\|\mathcal{H}\|_2$) can be found relatively easily, using the Levenberg−Marquardt algorithm, which works for arbitrary dimensions. In contrast, the Minimax solution is much harder to determine. In fact, to our knowledge, a generalization of the Remez algorithm to two (or even higher) dimensions does not exist.

Fortunately, the largest errors of $\mathcal{H}$ are on the diagonal $x = x'$, as can be seen in Figure 1. Therefore, it is a good approximation to consider the one-dimensional problems with the following error and model functions:

$$\eta(\vec{\gamma}, \vec{\nu}, x) = \frac{1}{x} - \frac{1}{\pi}\sum_{k=1}^N \gamma_k \phi^2(\nu_k, x) \tag{24}$$

$$\hat{\eta}(\vec{\sigma}, \vec{\tau}, x) = \frac{1}{2x} - \sum_{i=1}^N \sigma_i \hat{\phi}^2(\tau_i, x) \tag{25}$$

At this point, we note that the scaling relations of the coefficients between the cases $x \in [\varepsilon_{\min},\varepsilon_{\max}]$ and $x \in I = [1,R]$, with $R = \varepsilon_{\min}/\varepsilon_{\max}$, are trivial (primed coefficients correspond to $x \in [1,R]$):

$$\gamma_k' = \varepsilon_{\min}\gamma_k, \qquad \nu_k' = \varepsilon_{\min}\nu_k \tag{26}$$

$$\sigma_i' = \frac{\sigma_i}{2\varepsilon_{\min}}, \qquad \tau_i' = \frac{\tau_i}{2\varepsilon_{\min}} \tag{27}$$

dx.doi.org/10.1021/ct5001268 | J. Chem. Theory Comput. 2014, 10, 2498−2507

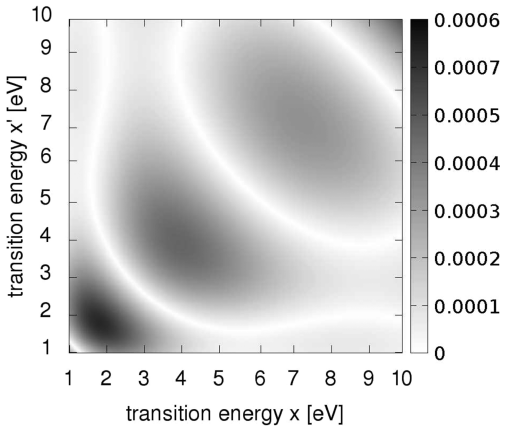

Figure 1. Least-squares error surface $|\mathcal{H}(\vec{\gamma}^0, \vec{\nu}^0, x, x')|$ measured in $[\mathrm{eV}^{-1}]$ for $\varepsilon_{\min} = 1$, $\varepsilon_{\max} = 10$, and $N = 3$. The largest errors are located along the diagonal $x = x'$.

Therefore, we can rely on the considerations of the previous section and minimize η and $\hat{\eta}$, with respect to either $\|\cdot\|_2$ or $\|\cdot\|_\infty$. This yields *least-squares* (γ_k^0,ν_k^0), (σ_i^0,τ_k^0) and *Minimax* (γ_k^*,ν_k^*), (σ_i^*,τ_i^*) quadratures for the frequency and time domain.

It is not entirely obvious, which integration method is preferable, but since the exact matrix elements χ_μ are not known a priori, a rigorous mathematical analysis suggests that the Minimax grid is superior.[40] If the density of the transition energies is considered, least-squares algorithms can become competitive to the Minimax algorithm.[10] Here, we have not considered these enhancements. A direct comparison between both methods for the time as well as the frequency domain can be found in section 3.

At the beginning of this section, we showed that the direct MP2 energy $E_c^{(2)}$, with the exact representations given by eqs 9, 11, and 18, can be seen as the first contribution to the RPA correlation energy (E_c^{RPA}, defined in eq 7). Now if $|E_c^{(n)}| < |E_c^{(2)}|$ for $n > 2$, the same must be true for the corresponding errors. In this case, we can expect that the quadrature error of eq 7 using least-squares or Minimax coefficients for the frequency domain is of the same order as for eq 19. Indeed, this is shown in section 3.

2.3. Nonuniform Cosine Transformation. In this section, we consider the duality of a given time and frequency grid for the polarizability. Assume that we have been given the polarizability $\hat{\chi}$ on a time grid, e.g., τ_i^*. Is it possible to compute the corresponding Fourier-transformed polarizability χ at frequency ν_k^* accurately without using an interpolation technique or increasing the number of quadrature points (N) significantly?

In order to answer this question, we first observe that the Fourier transform in our case reduces to a cosine transformation (cf. eqs 12 and 13). Second, we note that, generally, the Minimax grid points ν_k^*, τ_i^* are nonequally distributed. Thus, the vector $\{\chi_k^*\}_{k=1}^N$ cannot be written as a Z-transform of the vector $\{\hat{\chi}_i\}_{i=1}^N$ (as for fast Fourier transforms) and evaluation of the cosine transform in N ln(N) steps is not straightforward.[41] However, since, for our applications, the number of grid points is small ($N \leq 20$, cf. section 3), a computational cost of N^2 is not prohibitive, and we can evaluate the cosine integral directly. Therefore, we may reformulate our problem as follows: we seek a transformation matrix α_{ki} relating the vectors $\hat{\chi}_i$, χ_k by

$$\chi_k = \sum_{i=1}^{N} \alpha_{ki}\hat{\chi}_i \qquad \forall\ k = 1, ..., N \tag{28}$$

and, because of eq 12, we choose the following ansatz for α_{ki}:

$$\alpha_{ki} = \gamma_i^{(k)} \cos(\nu_k^*\tau_i^*) \tag{29}$$

Analogous to section 2.2, the coefficients $\gamma_i^{(k)}$ are determined only by the time and frequency dependence of $\hat{\chi}$ and χ. After inserting expressions for the polarizability in imaginary frequency (eq 14) and time (eq 15) into eq 28, we end up with the following error function at each frequency point ν_k^* for a specific energy difference $x \in [\varepsilon_{\min},\varepsilon_{\max}]$:

$$\eta^c(\vec{\gamma}^{(k)}, x) = \phi(\nu_k^*, x) - \sum_{i=1}^{N} \gamma_i^{(k)} \cos(\nu_k^*\tau_i^*)\hat{\phi}(\tau_i^*, x) \tag{30}$$

In contrast to section 2.1, now only the coefficients $\gamma_i^{(k)}$ are variational and the abscissas τ_i^* are kept fixed.

On the one hand, we found that η^c has more than $N + 1$ extrema x_j. This means that the system of eq 6 is overdetermined, which implies that the Remez algorithm from section 2.1 cannot be used.

On the other hand, the fitting problem is linear in $\gamma_i^{(k)}$. Consequently, we can find the least-squares solution in a stable way by using the singular value decomposition of the design matrix $D_{ij}^{(k)} = \cos(\nu_k^*\tau_i^*)\hat{\phi}(\tau_i^*,x_j)$. Hence, we may use the following *sloppy Remez algorithm*:[34]

(i) Choose one frequency point ν_k^*.
(ii) Find all extrema x_j of η^c.
(iii) Tabulate the deviations r_j from the median absolute deviation (MAD) r for each x_j.
(iv) Solve the overdetermined linear system of equations $\eta^c(\vec{\gamma}^{(k)}, x_j) + \mathrm{sgn}(r_j)r = 0$ for $\vec{\gamma}^{(k)}$ in the least-squares sense, i.e., find the minimum of

$$\left\|\eta^c(\vec{\gamma}^{(k)}, x) + \mathrm{sgn}(r - x)r\right\|_2$$

on the discrete set $x \in \{x_j\}$.
(v) Repeat steps (i)−(iv) until convergence is found.

This yields a set of coefficients $\gamma_i^{*(k)}$ for $i = 1, ..., N$ for a specific point ν_k^*.

The reader may have noticed that the procedure described above is applicable to any, arbitrary frequency point $\nu \in \mathbb{R}$. In principle, the set of coefficients $\{\gamma_i^{*(k)}\}_{k=1}^N$ can be considered to be a vector-valued function $\vec{\gamma}^*: \mathbb{R} \to \mathbb{R}^N$, $\nu \mapsto \vec{\gamma}^*(\nu)$ with the property that $\vec{\gamma}^*(\nu_k^*) = \vec{\gamma}^{*(k)}$. Hence, we can actually seek the (sloppy) Minimax solution $\|\eta^c(\nu)\|_\infty$ and vary the frequency ν continuously. We have done this for various Minimax time grids, i.e., for different values of R and N. In all cases, we found that the error $\|\eta^c(\nu)\|_\infty$ has a frequency dependence as shown in Figure 2. That is, for a time grid τ_i^*, the minima of $\|\eta^c(\nu)\|_\infty$ are exactly at the Minimax frequency points $\nu = \nu_k^*$.

Conversely, the transformation from the frequency grid to the time grid possesses a similar behavior: for a chosen Minimax frequency grid ν_k^*, the optimal time points of the inverse cosine error function,

$$\hat{\eta}^c(\vec{\sigma}(\tau), x) = \hat{\phi}(\tau, x) - \sum_{k=1}^{N} \sigma_k(\tau) \cos(\nu_k^*\tau)\phi(\nu_k^*, x) \tag{31}$$

are exactly at the Minimax time points τ_i^*, as shown in Figure 2b. Analogously, if the least-squares time grid τ_i^0 is chosen, one finds that ν_k^0 are the minima of the function min$\|\eta^c(\nu)\|_\infty$, and the converse holds for the back transformation. Therefore, we

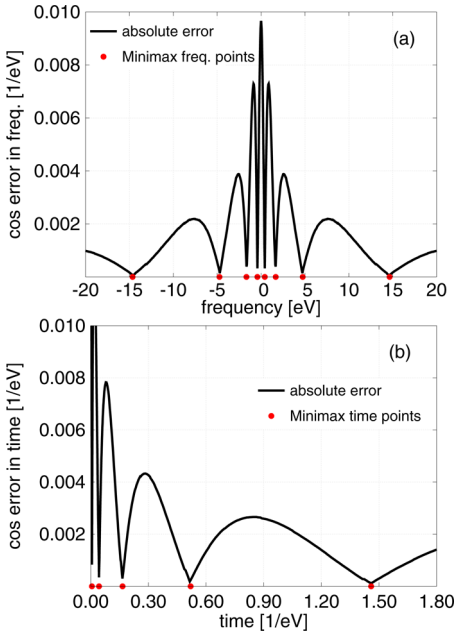

Figure 2. (a) Error of cosine transformation min $\|\eta^c\|_\infty$ as a function of the frequency ν for a Minimax time grid $\{\tau_i^*\}_{i=1}^N$ with transition energy ratio R = 100 and 5 grid points. (b) Transformation error in the time domain min $\|\hat{\eta}^c\|_\infty$ for the corresponding Minimax frequency grid. The error is minimal at the Minimax points ν_k^* in panel (a) and τ_i^* in panel (b) (red dots).

can make the statement that the two grid pairs $\{\nu_k^*\}_{k=1}^N,\{\tau_i^*\}_{i=1}^N$ and $\{\nu_k^0\}_{k=1}^N,\{\tau_k^0\}_{i=1}^N$ are *dual*, with respect to the cosine transformation. However, a rigorous mathematical proof is presently not known to us.

2.4. Cubic Scaling RPA Algorithm. In this section, we discuss the application of the results of the previous sections (sections 2.2 and 2.3) to the efficient computation of the RPA correlation energy (eq 7), using imaginary time Green's functions. Typical RPA codes scale like M^4 (where M is a measure for the system size), so that currently RPA calculations for large systems are computationally expensive and, therefore, are limited to a few hundred electrons.[21−25,38] The computational bottleneck of most RPA implementations is the direct calculation of the independent particle polarizability χ, using, for instance, eq 14, which, by itself, is an $O(NM^4)$ step (where N is the number of frequency grid points).

Nevertheless, as mentioned in section 1, the computational cost and complexity can be reduced to NM^3 by using the (noninteracting) single particle Green's function (G) in imaginary time:[30,33]

$$G(\mathbf{r},\mathbf{r}',i\tau) = \Theta(\tau)\sum_a \varphi_a(\mathbf{r})\varphi_a^*(\mathbf{r}')e^{-(\varepsilon_a-\varepsilon_F)\tau} - \Theta(-\tau)\sum_i \varphi_i(\mathbf{r})\varphi_i^*(\mathbf{r}')e^{-(\varepsilon_i-\varepsilon_F)\tau} \quad (32)$$

Here, Θ is the Heaviside step function, ε_F is the Fermi energy, φ_a (φ_i) is an unoccupied (occupied) one-electron orbital with energy ε_a (ε_i), and $\mathbf{r},\mathbf{r}'$ are real lattice vectors. For a periodic system, the identity

$$G(\mathbf{r}+\mathbf{R},\mathbf{r}'+\mathbf{R},i\tau) = G(\mathbf{r},\mathbf{r}',i\tau) \quad (33)$$

holds for arbitrary lattice translation vectors $\mathbf{R}$. This implies that the computation of G at all considered frequency points is essentially an NM^3 step. Once G is determined, we can use the well-known product formula (eq 2) to obtain the independent particle polarizability in real space and imaginary time $\hat{\chi}(\mathbf{r},\mathbf{r}',i\tau)$. In order to calculate the RPA energy from eq 7, one needs the polarizability in the reciprocal space at imaginary frequencies. The Fourier transformation, with respect to the lattice, is obtained by a fast Fourier transformation

$$\hat{\chi}_{\mathbf{G}\mathbf{G}'}(\mathbf{q},i\tau) = \sum_{\mathbf{r}\mathbf{r}'} e^{-i(\mathbf{G}+\mathbf{q})\mathbf{r}}\hat{\chi}(\mathbf{r},\mathbf{r}',i\tau)e^{i(\mathbf{G}'+\mathbf{q})\mathbf{r}'} \quad (34)$$

where $\mathbf{G},\mathbf{G}'$ are reciprocal lattice vectors and $\mathbf{q}$ is a vector in the first Brillouin zone. This step scales like $NM^2\ln(M)$. What remains to be performed is the forward cosine transformation defined in eq 12 in order to get $\chi_{\mathbf{G}\mathbf{G}'}(\mathbf{q},i\nu)$ scaling like $N^2M^2\ln(M)$. Finally, the RPA energy is obtained by[44]

$$E_c^{\mathrm{RPA}} = \frac{1}{2\pi N_{\mathbf{q}}}\sum_{\mathbf{G}\mathbf{q}}\sum_{k=1}^{N}\gamma_k\{\ln[1-\chi V]_{\mathbf{G}\mathbf{G}'}(\mathbf{q},i\nu_k) - \chi_{\mathbf{G}\mathbf{G}}(\mathbf{q},i\nu_k)V_{\mathbf{G}\mathbf{G}}(\mathbf{q})\} \quad (35)$$

Here, $N_{\mathbf{q}}$ is the number of sample points in the first Brillouin zone and $V_{\mathbf{G}\mathbf{G}}(\mathbf{q})$ is the Coulomb potential in reciprocal space at the wave vector $\mathbf{q}$ in the first Brillouin zone. If M is the number of considered reciprocal lattice vectors $\mathbf{G}$ and $N \ll M$, the procedure described above scales in total like $NM^3 \approx M^3$.

Because the error of the total energy grows linearly with the system size M, it might be necessary to increase the number of quadrature points N. However, since the integration algorithms considered here are exponentially converging, the necessary number of quadrature points N grows, at most, like ln M; in fact, even for large systems, more than 20 frequency and time points will be hardly ever required. Details of the implementation for the bulk with a finite Brillouin zone sampling will be presented elsewhere.[45]

In the following sections, we show the convergence behavior of the Minimax and least-squares grids for MP2 as well as the RPA correlation energy and investigate the accuracy of the nonuniform cosine transformation.

2.5. Technical Details. We have implemented the required code to calculate the least-squares and Minimax grids for both the imaginary frequency and time domain in VASP.[42,43]

For the calculation of the least-squares grid, the nonlinear fitting problem (discussed in section 2.1) is solved using the Levenberg−Marquardt algorithm[34] after the starting guesses for $(\vec{\gamma}^0,\vec{\nu}^0),(\vec{\sigma}^0,\vec{\tau}^0)$ are initialized randomly. This is done for $R = \varepsilon_{\max}/\varepsilon_{\min}$. The resulting coefficients are then scaled for the proper interval $[\varepsilon_{\min},\varepsilon_{\max}]$ using the relationships described by eq 26.

For the Minimax grid, we have implemented a Remez algorithm, which is capable of calculating the quadratures $(\vec{\gamma}^*,\vec{\nu}^*),(\vec{\sigma}^*,\vec{\tau}^*)$ for a given $N \le 20$. Our present implementation is limited to N = 20, since the Remez algorithm is numerically ill-conditioned using double precision LAPACK routines. First, the code determines $R = \varepsilon_{\max}/\varepsilon_{\min}$ and reads pretabulated Minimax coefficients for the next smaller value of R from a table. These are used as starting values for the setup of the corresponding error function. In the next step, the absolute maximum ε of η (respectively $\hat{\eta}$) in $[1,R]$ and the x_j (set of all local extrema including the boundaries 1 and R in $[1,R]$) are determined. Finally, the nonlinear set of eqs 6 is solved using a standard damped Newton−Raphson algorithm and the procedure is iterated until convergence is reached.

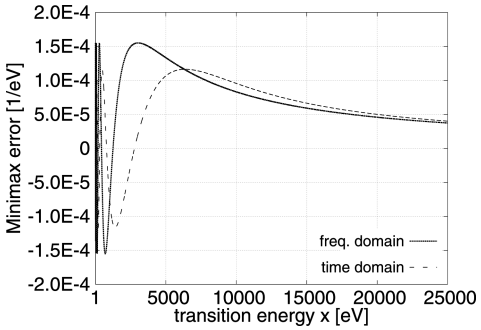

Figure 3. Minimax error functions for the time $\hat{\eta}$ (solid line) and frequency η (dashed line) domain for $R_7 = 28387$ and $N = 7$. Both functions decay strictly for $x > R_7$.

We note that, for any given N, an upper bound R_N exists, so that the corresponding error functions $\eta(x)$, $\hat{\eta}(x)$ decay strictly for all $x > R_N$. Figure 3 shows an example of this case. If, for a given N, the transition energy ratio R is larger than R_N, the error is minimized in the interval $[1,R_N]$ instead of $[1,R]$, because the total error for both intervals coincide (see ref 40 for more details). [We thank Wolfgang Hackbusch, who provided us with the Minimax starting table for the time domain. The values of R_N are available online at http://www.mis.mpg.de/scicomp/EXP_SUM/1_x/tabelle.]

The convergence behavior of the cosine transform (eq 28) is tested by first calculating the polarizability on an imaginary time grid and then performing the cosine transform. The code first determines the coefficients $\gamma_i^{*(k)}$ by minimizing the error function 30 using the *sloppy Remez algorithm* (cf. section 2.3). In the next step the polarizability, $\hat{\chi}$ is evaluated at the Minimax time grid τ_i^* and the cosine transform is calculated using eq 28 with $\alpha_{ki} = \gamma_i^{*(k)} \cos(\nu_k^*,\tau_i^*)$. In the final step, the RPA correlation energy E_c^{RPA} is calculated with eq 35 using the Minimax quadrature $\{\nu_k^*,\gamma_k^*\}$ for the frequency integral in eq 7. For the evaluation of $\ln(1 - \chi V)$, the method described in ref 44 is applied. The same procedure is tested for the least-squares quadrature $\{\nu_k^0, \gamma_k^0\}$ as well.

3. RESULTS

3.1. Results for ZnO and Si. We have calculated the RPA and direct MP2 energies of zinc-blende ZnO and fcc Si using lattice constants of $a = 4.58$ Å and $a = 5.43$ Å, respectively. The Brillouin zone was sampled with $4 \times 4 \times 4$ k-points (including the Γ-point) and the sum over **G**-vectors and bands in the polarizability were restricted to an energy cutoff of 250 eV and 256 eV bands, respectively.

These two examples are representative of cases, where the number of valence-conduction band pairs is on the order of several millions, so that standard MP2 algorithms are already exceedingly expensive and (at least with our code) hardly doable. However, the single particle gap is sizable in both cases, and does not pose a significant challenge to the numerical quadrature.

Table 1 reports results for the direct MP2 energy $E_c^{(2)}$ of ZnO calculated using an imaginary time and imaginary frequency grid. Here, the polarizabilities were calculated directly on the imaginary time and imaginary frequency axis, respectively (not applying cosine transformations). We found that, for both the least-squares method as well the Minimax grid, the direct MP2 contribution can be evaluated with an accuracy of 1 meV with only 8 quadrature points. Note that these calculations were performed using density functional theory (DFT) orbitals and one-electron energies (as opposed to the conventionally used Hartree−Fock orbitals). The imaginary time integration converges slightly faster than the frequency integration. This is related to larger errors in the frequency domain, as one can see from Figures 4a and 4b.

Table 1. Convergence of Direct MP2 Energy $E_c^{(2)}$ for the Least Squares (LS) and Minimax (MM) Quadratures for ZnO[a]

	Imaginary Time Quadrature		Imaginary Frequency Quadrature	
N	MM	LS	MM	LS
6	−38.724 565	−38.712 628	−38.761 542	−38.728 091
7	−38.717 135	−38.719 412	−38.724 606	−38.717 356
8	−38.721 148	−38.721 509	−38.720 937	−38.721 975
9	−38.721 577	−38.721 660	−38.721 925	−38.721 735
10	−38.721 763	−38.721 812	−38.721 696	−38.721 787
11	−38.721 770	−38.721 772	−38.721 754	−38.721 754
12	−38.721 768	−38.721 769	−38.721 762	−38.721 762
13	−38.721 767	−38.721 767	−38.721 768	−38.721 769
14	−38.721 767	−38.721 765	−38.721 767	−38.721 765
15	−38.721 767	−38.721 767	−38.721 767	−38.721 770
16	−38.721 767	−38.721 768	−38.721 767	−38.721 764
17	−38.721 767	−38.721 768	−38.721 767	−38.721 769
18	−38.721 767	−38.721 767	−38.721 767	−38.721 767
19	−38.721 767	−38.721 767	−38.721 767	−38.721 767
20	−38.721 767	−38.721 767	−38.721 767	−38.721 767

[a]Columns 2 and 3 contain $E_c^{(2)}$ evaluated on the imaginary time axis (using eq 20), whereas the values in columns 4 and 5 are obtained with an imaginary frequency integration (using eq 19).

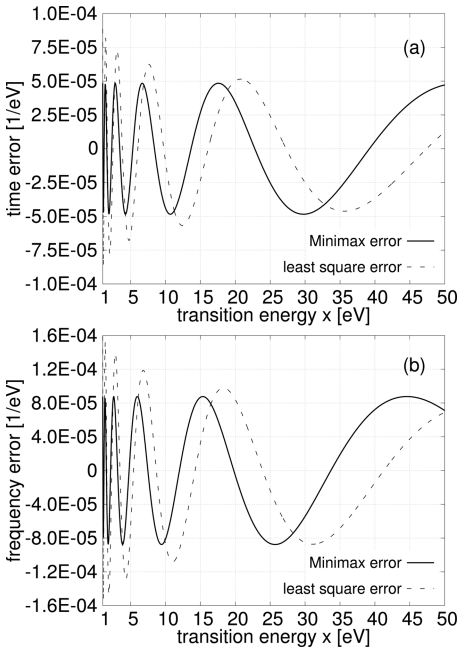

Figure 4. Minimax and least-squares error functions for $R = 500$ and $N = 7$ in the (a) time and (b) frequency domain. For small x (dominating terms in χ and $\hat{\chi}$), the Minimax solution is more accurate.

From a direct comparison of the Minimax with the least-squares grid (columns 2 and 3, respectively (columns 4 and 5 in Table 1)) one clearly sees that the Minimax quadrature achieves 1 μeV precision already around 13 grid points, whereas the same accuracy with residual fluctuations of few μeV is

dx.doi.org/10.1021/ct5001268 | J. Chem. Theory Comput. 2014, 10, 2498−2507

hardly obtained using the least-squares quadrature. [The convergence of the least-squares grid can be improved by accounting for appropriate distributions $p(x) \neq 1$ of the transition energies x. Reference 10 shows that the resulting quadrature is competitive with the Minimax solution of the fitting problem with $p(x) = 1$.] This is in accordance with ref 10, where the Minimax and the least-squares quadrature for benzene was investigated. The excellent convergence of the Minimax quadrature is not surprising. As shown in Figure 4, the Minimax solution is more accurate by a factor of ∼2 for small values of x (corresponding to small transition energies, i.e., dominating terms in χ and $\hat{\chi}$). However, Tables 2 and 3 show that the least-squares grid performs reasonably well for the RPA, although, again, the Minimax has a slight edge, in particular, for Si. In fact, the RPA energy converges slightly faster than the MP2 energy for ZnO (compare columns 2 and 3 in Table 2 to columns 4 and 5 in Table 1). It can be seen that μeV accuracy in E_c^{RPA} is reached with 14 points using the least-squares grids, which is only one point more than the number of points required in the Minimax grid, and less than for the least-squares grid in the MP2 case. The main reason for this is that the RPA dampens and reduces the contributions from low-energy transitions since $\ln(1 - x) + x < -x^2/2$ for all $x < 1$. [This follows trivially by expanding $\ln(1 - x)$ into a power series.]

Table 2. RPA Correlation Energies E_c^{RPA} of ZnO; Convergence of the Energy, with Respect to the Number of Grid Points (N), is Studied for Least Squares (LS) and Minimax (MM) Quadratures[a]

	RPA Correlation Energy, E_c^{RPA} (meV)			
	$\chi(\nu_k)$		$\hat{\chi}(\tau_i) \rightarrow \chi(\nu_k)$	
N	MM	LS	MM	LS
6	−22.170 380	−22.097 279	−22.099 078	−22.085 478
7	−22.112 212	−22.104 315	−22.107 192	−22.120 936
8	−22.108 687	−22.109 619	−22.110 301	−22.106 798
9	−22.109 932	−22.109 877	−22.110 571	−22.111 472
10	−22.109 903	−22.109 894	−22.110 062	−22.109 677
11	−22.109 920	−22.109 924	−22.109 929	−22.109 843
12	−22.109 923	−22.109 930	−22.109 917	−22.109 863
13	−22.109 929	−22.109 930	−22.109 914	−22.109 908
14	−22.109 929	−22.109 928	−22.109 926	−22.109 950
15	−22.109 929	−22.109 929	−22.109 926	−22.109 939
16	−22.109 929	−22.109 929	−22.109 933	−22.109 925
17	−22.109 929	−22.109 929	−22.109 930	−22.109 932
18	−22.109 929	−22.109 929	−22.109 927	−22.109 927
19	−22.109 929	−22.109 929	−22.109 929	−22.109 929
20	−22.109 929	−22.109 929	−22.109 929	−22.109 929

[a]In columns 2 and 3, the polarizabilities are calculated directly on the imaginary frequency axis. In columns 4 and 5, the polarizabilities are determined by cosine transformations from the time axis to the frequency axis.

Table 3. RPA Correlation Energies (E_c^{RPA}) of Si[a]

	RPA Correlation Energy, E_c^{RPA} (meV)			
	$\chi(\nu_k)$		$\hat{\chi}(\tau_i) \rightarrow \chi(\nu_k)$	
N	MM	LS	MM	LS
6	−16.899 448	−16.818 975	−16.824 963	−16.757 714
7	−16.772 977	−16.733 343	−16.745 291	−16.729 756
8	−16.726 807	−16.721 862	−16.726 670	−16.728 531
9	−16.723 844	−16.724 469	−16.726 550	−16.725 981
10	−16.725 207	−16.725 417	−16.725 633	−16.725 277
11	−16.725 563	−16.725 468	−16.725 678	−16.725 643
12	−16.725 582	−16.725 515	−16.725 718	−16.725 669
13	−16.725 587	−16.725 560	−16.725 643	−16.725 633
14	−16.725 589	−16.725 576	−16.725 608	−16.725 605
15	−16.725 589	−16.725 583	−16.725 596	−16.725 597
16	−16.725 589	−16.725 586	−16.725 587	−16.725 591
17	−16.725 589	−16.725 588	−16.725 588	−16.725 589
18	−16.725 589	−16.725 589	−16.725 589	−16.725 589
19	−16.725 589	−16.725 589	−16.725 589	−16.725 589
20	−16.725 589	−16.725 589	−16.725 589	−16.725 589

[a]See Table 2 for details.

We have also investigated the accuracy of the nonuniform cosine transform described in section 2.3. The results for the RPA correlation energy for the Minimax and least-squares grids are given in columns 4 and 5 of Tables 2 and 3. It can be seen that the cosine transformation of $\hat{\chi}(i\tau_i)$ can be carried out with little loss of accuracy, i.e., convergence of E_c^{RPA} within 1 meV (1 μeV) is achieved for 10 (19) grid points. When the polarizability is calculated via a cosine transformation, both grids show the same convergence, so that the Minimax grid is not superior to the least-squares grid when the polarizability is evaluated in imaginary time and subsequently Fourier-transformed. This is most likely related to the fact that the nonuniform cosine coefficients $\gamma_i^{*(k)}$ are obtained from the solution of a least-squares fitting problem (cf. section 2.3). Although use of the cosine transform requires slightly more frequency points, this is usually more than compensated by the greatly reduced time complexity and lower scaling of the corresponding approach.

A final remark is given here. For Si, the 3s and 3p states, and, for ZnO, the Zn 3d, O 2s, and O 2p states are treated as valence electrons, yielding a minimization interval of [1,525] for the former and [1,470] for the latter. This results in the good grid convergence shown in Tables 1, 2, and 3. In the presence of shallow core electrons, the minimization intervals will increase slightly, since the core electrons lie typically 100−200 eV lower in the energy than the valence electrons. This will not deteriorate the grid convergence considerably, because the presented integration method converges exponentially with the number of grid points.

3.2. Results for the Al and Nb Atoms. From the previous discussion, it is clear that the convergence of RPA energies for systems with small gaps is harder to achieve, since a small gap will necessarily increase the width of the interval onto which we map [1,R]. For vanishing or zero gap, the direct MP energies tend to diverge $E_c^{(n)} \rightarrow \infty$, whereas the RPA energy ($E_c^{\mathrm{RPA}} = \sum_{n=0}^{\infty} E_c^{(n)}$) usually remains finite.[46] Hence, we consider only the RPA correlation energy in this section.

We have studied the convergence of the Minimax grid and the corresponding nonuniform cosine transformation for atomic Al and Nb. Both atoms are characterized by a tiny one-electron gap in DFT when the Perdew−Burke−Ernzerhof (PBE) functional is used.[47,48] For Al, for instance, a symmetry-broken solution is found where the three (degenerate) p-orbitals split into one occupied and two unoccupied states separated by an energy difference of 10 meV. Analogously, for Nb, the one-electron Kohn−Sham gap is ∼90 meV, so that we can consider both, the Al and Nb atom as particularly challenging model systems for small gap systems. Note that the exact magnitude of the one-electron gap might vary between different implementations and box sizes; however, this is irrelevant for the present case, since we only want to

dx.doi.org/10.1021/ct5001268 | J. Chem. Theory Comput. 2014, 10, 2498−2507

demonstrate that reasonably accurate answers can be obtained, even in such problematic cases.

The calculations of the RPA correlation energies were done at the Γ-point only in a cell with dimensions of 7 Å × 8 Å × 9 Å. An energy cutoff of 250 eV for Al and 286 eV for Nb was chosen. The sum over bands for the polarizability was restricted to 8000 for Al and to 10 800 for Nb, respectively. The convergence of the Minimax frequency quadrature and the cosine transformation are shown in Table 4.

Table 4. RPA Correlation Energy (E_c^{RPA}) of Atomic Al and Nb for Minimax Integration[a]

	RPA Correlation Energy E_c^{RPA} (meV)			
	Al		Nb	
N	$\chi(\nu_k^*)$	$\chi(\tau_i^*) \rightarrow \chi(\nu_k^*)$	$\chi(\nu_k^*)$	$\chi(\tau_i^*) \rightarrow \chi(\nu_k^*)$
8	−3.961 488	−3.748 070	−18.620 212	−18.188 877
9	−5.589 998	−5.734 705	−18.505 670	−18.363 117
10	−5.960 436	−6.369 540	−18.429 473	−18.413 159
11	−6.782 374	−6.802 507	−18.431 352	−18.437 847
12	−6.857 853	−6.773 977	−18.436 204	−18.439 505
13	−6.749 695	−6.729 153	−18.438 163	−18.439 723
14	−6.719 201	−6.720 474	−18.439 045	−18.439 421
15	−6.720 629	−6.724 039	−18.438 764	−18.439 353
16	−6.723 408	−6.726 318	−18.438 671	−18.438 573
17	−6.724 243	−6.726 230	−18.438 669	−18.438 614
18	−6.724 488	−6.725 019	−18.438 664	−18.438 665
19	−6.724 500	−6.724 629	−18.438 668	−18.438 664
20	−6.724 518	−6.724 485	−18.438 670	−18.438 682

[a]In columns 2 and 4, the polarizabilities are calculated directly on the imaginary frequency axis, whereas in columns 3 and 5, the polarizabilities are determined by cosine transformations from the time axis to the frequency axis.

One clearly recognizes that the accuracy for the Al and Nb atoms is poor, compared to that for ZnO and Si. In order to obtain results with similar accuracy, for Nb, we need approximately twice as many grid points (N = 15) as those needed for the semiconductors, and for Al, even a denser grid is necessary (N = 17). Still, for Nb, at least μeV precision can be reached with $N \approx 20$ frequency points. When the response function is calculated first in imaginary time and then cosine-transformed, again, as in the case of the semiconductors, we observe that meV accuracy is reached by using slightly denser grids (19 for Al and 16 for Nb). However, even at 20 grid points, a residual error of 10 μeV and 100 μeV prevails for the Nb atom and Al atom, respectively.

The reason for this behavior is the large minimization interval (R = 47 143 for Al and R = 5390 for Nb) required to also capture very small energy transitions in the polarizability. This is also indicated by the slightly better convergence of Nb, because of a smaller value of R, compared to that of Al.

Although the necessity of dense grids for small gap systems is not surprising, we believe that grids on the order $N \approx 20$ for accurate RPA energies of systems with gaps between 10 meV and 100 meV are acceptable.

4. CONCLUSION

In this paper, we have investigated the possibility to develop an RPA algorithm scaling cubically with system size M. An outline of the algorithm was presented in section 1. It is based on the space-time GW method of Rojas et al.[30] First, the noninteracting Green's function $G(i\tau)$ (defined in eq 32) is evaluated on an imaginary time grid τ_i. Then, the well-known equation for the independent particle polarizability $\hat{\chi}(i\tau_i)$ (eq 2) is used. Subsequently, a cosine transformation of the latter yields the polarizability at imaginary frequencies $\chi(i\nu_k)$, so that the ACFD theorem (eq 35) can be used. In sections 1 and 2.4, we have pointed out that this algorithm will benefit from optimized imaginary time and frequency grids that keep the number of grid points small.

In order to achieve this goal, we have used nonequally spaced grids based on quadratures for the RPA integral described by eq 7 and its lowest order contribution, the direct MP2 energy $E_c^{(2)}$. Since the latter can be evaluated efficiently on the imaginary time as well as the imaginary frequency axis, we have first focused our attention on the MP2 integral representations in imaginary time (eq 11) and imaginary frequency (eq 9).

The construction of imaginary time quadratures is a well-studied problem and appears in Laplace-transformed Møller–Plesset (LP-MP) perturbation theory. Here, we compared Minimax and least-squares quadratures, finding that the former is slightly superior for the materials considered here (see section 3.1).

To evaluate the RPA correlation energy using eq 7, an imaginary frequency quadrature is needed. In order to obtain accurate frequency grids, we have proceeded analogously to the construction of the time grid, i.e., we have minimized the quadrature error of the imaginary frequency representation (eq 9) of the direct MP2 energy. In section 3, we have shown that the resulting frequency quadratures can be used for an accurate frequency integration of the MP2 and RPA energies. For gapped systems, such as ZnO and Si, the Minimax quadrature is again slightly better than the least-squares grid reaching μeV accuracy of $E_c^{(2)}$ and E_c^{RPA} at ∼13 frequency points (cf. section 3.1).

Furthermore, in section 3.2, we have briefly explained the challenge of determining E_c^{RPA} for small-gap systems. Because of the existence of tiny transition energies in the independent particle polarizability $\chi(i\nu)$, more grid points are necessary for an accurate frequency integration. We have seen that, for systems with band gaps of a few tens of meV (atomic Al and Nb), meV accuracy of E_c^{RPA} is only attained at ∼16 grid points.

The main achievement of the present work is the numerical cosine transformation of the polarizability from the imaginary time to the imaginary frequency axis presented in section 2.3. We have approximated the cosine integral described by eq 12 by a discrete sum and subsequently minimized the corresponding error (eq 30). This gives rise to a nonuniform cosine transformation, allowing for an accurate switching between imaginary time and frequency polarizabilities without using an interpolation technique or increasing the number of grid points N significantly. Since the computational time, as well as the working memory, are linearly dependent on N, an optimized frequency and time grid helps to reduce the storage and the computational cost of the low scaling RPA algorithm discussed in section 2.4.

Remarkably, we observe a strict "duality" between the Minimax time and frequency grids: i.e., for a given Minimax time grid, errors due to the cosine transform are minimal at the Minimax frequency points, and vice versa. Initially, this duality may appear to be somewhat unexpected. For instance, the small frequencies present on the frequency grid imply rapid oscillations as a function of time, and one might then ask why coarse grids at large imaginary times are sufficient and optimal to

represent such oscillations. We have no formal mathematical justification for that observation. However, one should keep in mind that, in imaginary time τ, a transition at the energy x on the real axis results in an exponentially decaying function $\exp(-\tau x)$. The corresponding functions in imaginary frequency ν are decaying rational functions of the form $x/(x^2 + \nu^2)$. None of these functions are oscillatory: they are smooth and decay toward zero at infinite (imaginary) time and frequency. The spacing of the time and frequency grids are most likely optimal to represent such functions.

We have investigated the convergence of the cosine transform with respect to the number of time and frequency grid points in section 3. For Si and ZnO, the transformation of $\hat{\chi}(i\tau_i) \rightarrow \chi(i\nu_k)$ and subsequent calculation of the RPA correlation energy can be performed with meV (μeV) accuracy with 10 (19) grid points. An accuracy of ∼1 meV for systems with a tiny one electron gap, such as the Al and Nb atoms, is reached at ∼16 grid points, and with 20 grid points, the error approaches ∼10 μeV. This should be adequate for most materials and is small, compared to errors incurred by the random phase approximation (RPA) itself. To achieve the same accuracy, the cosine-transformation-based algorithm requires ∼20%−30% more time and frequency points than a direct calculation of the polarizability on the frequency grid. This is a modest penalty, which is more than compensated by the improved scaling. Details of the RPA code scaling cubically with the system size using the cosine transformation developed here will be presented in a future work.[45]

AUTHOR INFORMATION

Corresponding Author

*E-mail: merzuk.kaltak@univie.ac.at.

Notes

The authors declare no competing financial interest.

ACKNOWLEDGMENTS

This work was supported by the Austrian Spezialforschungsbereich Vienna Computational Materials Laboratory (SFB ViCoM) and the Deutsche Forschungsgruppe Research Unit FOR 1346.

REFERENCES

(1) Møller, C.; Plesset, M. S. Note on an Approximation Treatment for Many-Electron Systems. *Phys. Rev.* **1934**, *46*, 618−622.
(2) Almlöf, J. Elimination of energy denominators in Møller—Plesset perturbation theory by a Laplace transform approach. *Chem. Phys. Lett.* **1991**, *181*, 319−320.
(3) Häser, M.; Almlöf, J. Laplace transform techniques in Møller−Plesset perturbation theory. *J. Chem. Phys.* **1992**, *96*, 489−494.
(4) Izmaylov, A. F.; Scuseria, G. E. Resolution of the identity atomic orbital Laplace transformed second order Møller−Plesset theory for nonconducting periodic systems. *Phys. Chem. Chem. Phys.* **2008**, *10*, 3421−3429.
(5) Doser, B.; Lambrecht, D. S.; Ochsenfeld, C. Tighter multipole-based integral estimates and parallel implementation of linear-scaling AO-MP2 theory. *Phys. Chem. Chem. Phys.* **2008**, *10*, 3335−3344.
(6) Ayala, P. Y.; Scuseria, G. E. Linear scaling second-order Møller−Plesset theory in the atomic orbital basis for large molecular systems. *J. Chem. Phys.* **1999**, *110*, 660−3671.
(7) Kats, D.; Usvyat, D.; Schütz, M. On the use of the Laplace transform in local correlation methods. *Phys. Chem. Chem. Phys.* **2008**, *10*, 3430−3439.
(8) Takatsuka, A.; Ten-no, S.; Hackbusch, W. Minimax approximation for the decomposition of energy denominators in Laplace-transformed Møller-Plesset perturbation theories. *J. Chem. Phys.* **2008**, *129*, 044112.
(9) Braess, D. *Nonlinear Approximation Theory*; Springer Series in Computational Mathematics; Springer−Verlag: Berlin, Heidelberg, 2011
(10) Kats, D.; Usvyat, D.; Loibl, S.; Merz T.; Schütz, M. Comment on "Minimax approximation for the decomposition of energy denominators in Laplace-transformed Møller−Plesset perturbation theories". *J. Chem. Phys.* **2009**, *130*.
(11) Furche, F.; Van Voorhis, T. Fluctuation−dissipation theorem density-functional theory. *J. Chem. Phys.* **2005**, *122*, 164106.
(12) Furche, F. Molecular tests of the random phase approximation to the exchange-correlation energy functional. *Phys. Rev. B* **2001**, *64*, 195120.
(13) Langreth, D. C.; Perdew, J. P. Exchange-correlation energy of a metallic surface: Wave-vector analysis. *Phys. Rev. B* **1977**, *15*, 2884−2901.
(14) Marini, A.; Garcia-Gonzalez, P.; Rubio, A. First-principles description of correlation effects in layered materials. *Phys. Rev. Lett.* **2006**, *96*, 136404.
(15) Miyake, T.; Aryasetiawan, F.; Kotani, T.; van Schilfgaarde, M.; Usuda, M.; Terakura, K. Total energy of solids: An exchange and random-phase approximation correlation study. *Phys. Rev. B* **2002**, *66*, 245103.
(16) Ren, X.; Rinke, P.; Tkatchenko, A.; Scheffler, M. Beyond the Random-Phase Approximation for the Electron Correlation Energy: The Importance of Single Excitations. *Phys. Rev. Lett.* **2011**, *106*, 153003.
(17) Marsman, M.; Grüneis, A.; Paier, J.; Kresse, G. Second-order Moeller-Plesset perturbation theory applied to extended systems. I. Within the projector-augmented-wave formalism using a plane wave basis set. *J. Chem. Phys.* **2009**, *130*, 184103.
(18) Schimka, L.; Harl, J.; Stroppa, A.; Grüneis, A.; Marsman, M.; Mittendorfer, F.; Kresse, G. Accurate surface and adsorption energies from many-body perturbation theroy. *Nat. Mater.* **2010**, *9*, 741−744.
(19) Feibelman, P. J.; Hammer, B.; Norskov, J. K.; Wagner, F.; Scheffler, M.; Stumpf, R.; Watwe, R.; Dumesic, J. The CO/Pt(111) puzzle. *J. Phys. Chem. B* **2001**, *105*, 4018.
(20) Schimka, L.; Gaudoin, R.; Klimeš, J.; Marsman, M.; Kresse, G. Lattice constants and cohesive energies of alkali, alkaline-earth, and transition metals: Random phase approximation and density functional theory results. *Phys. Rev. B* **2013**, *87*, 214102.
(21) Olsen, T.; Thygesen, K. S. Random phase approximation applied to solids, molecules, and graphene-metal interfaces: From van der Waals to covalent bonding. *Phys. Rev. B* **2013**, *87*, 075111.
(22) Eshuis, H.; Furche, F. A Parameter-Free Density Functional That Works for Noncovalent Interactions. *J. Phys. Chem. Lett.* **2011**, *2*, 983−989.
(23) Eshuis, H.; Yarkony, J.; Furche, F. Fast computation of molecular random phase approximation correlation energies using resolution of the identity and imaginary frequency integration. *J. Chem. Phys.* **2010**, *132*, 234114.
(24) Ren, X.; Rinke, P.; Blum, V.; Wieferink, J.; Tkatchenko, A.; Sanfilippo, A.; Reuter, K.; Scheffler, M. Resolution-of-identity approach to Hartree-Fock, hybrid density functionals, RPA, MP2 and GW with numeric atom-centered orbital basis functions. *New J. Phys.* **2012**, *14*, 053020.
(25) Harl, J.; Kresse, G. Accurate Bulk Properties from Approximate Many-Body Techniques. *Phys. Rev. Lett.* **2009**, *103*, 056401.
(26) Wiser, N. Dielectric Constant with Local Field Effects Included. *Phys. Rev.* **1963**, *129*, 62−69.
(27) Adler, S. L. Quantum Theory of the Dielectric Constant in Real Solids. *Phys. Rev.* **1962**, *126*, 413−420.
(28) Shishkin, M.; Kresse, G. Self-consistent GW calculations for semiconductors and insulators. *Phys. Rev. B* **2007**, *75*, 235102.
(29) Hedin, L. New Method for Calculating the One-Particle Green's Function with Application to the Electron-Gas Problem. *Phys. Rev.* **1965**, *139*, A796−A823.

(30) Rojas, H. N.; Godby, R. W.; Needs, R. J. Space-Time Method for *Ab Initio* Calculations of Self-Energies and Dielectric Response Functions of Solids. *Phys. Rev. Lett.* **1995**, *74*, 1827−1830.
(31) Foerster, D.; Koval, P.; Sánchez-Portal, D. An $O(N^3)$ implementation of Hedin's *GW* approximation for molecules. *J. Chem. Phys.*, *140*,014107, Jan **2014**.
(32) Moussa, J. E. Cubic-scaling algorithm and self-consistent field for the random-phase approximation with second-order screened exchange. *J. Chem. Phys.* **2014**, *140*, 014107.
(33) Steinbeck, L.; Rubio, A.; Reining, L.; Torrent, M.; White, I. D.; Godby, R. W. Enhancements to the GW space-time method. *Comput. Phys. Commun.* **2000**, *125*, 105−118.
(34) Press, W. H.; Teukolsky, S. A.; Vetterling, W. T.; Flannery, B. P. *Numerical Recipes: The Art of Scientific Computing*, 3rd Edition; Cambridge University Press: Oxford, U.K., 2007.
(35) Remez, E. Ya *General computational methods of Chebyshev approximation: The problems with linear real parameters*; U.S. Atomic Energy Commission, Division of Technical Information: Washington, DC, 1962.
(36) Gell-Mann, M.; Brueckner, K. A. Correlation Energy of an Electron Gas at High Density. *Phys. Rev.* **1957**, *106*, 364−368.
(37) Onida, G.; Reining, L.; Rubio, A. Electronic excitations: Density-functional versus many-body Green's-function approaches. *Rev. Mod. Phys.* **2002**, *74*, 601−659.
(38) Furche, F. Developing the random phase approximation into a practical post-Kohn−Sham correlation model. *J. Chem. Phys.* **2008**, *129*, 114105.
(39) Wilson, A. K.; Almlöf, J. Møller−Plesset correlation energies in a localized orbital basis using a Laplace transform technique. *Theor. Chim. Acta* **1997**, *95*, 49−62.
(40) Braess, D.; Hackbusch, W. Approximation of $1/x$ by exponential sums in $[1,\infty)$. *IMA J. Numer. Anal.* **2005**, *25*, 685−697.
(41) Dutt, A.; Rokhlin, V. Fast Fourier Transforms for Non-equispaced Data. *SIAM J. Sci. Comput.* **1993**, *14*, 1368−1393.
(42) Kresse, G.; Hafner, J. *Ab initio* molecular dynamics for liquid metals. *Phys. Rev. B* **1993**, *47*, 558−561.
(43) Kresse, G.; Joubert, D. From ultrasoft pseudopotentials to the projector augmented-wave method. *Phys. Rev. B* **1999**, *59*, 1758−1775.
(44) Harl, J.; Kresse, G. Cohesive energy curves for noble gas solids calculated by adiabatic connection fluctuation-dissipation theory. *Phys. Rev. B* **2008**, *77*, 045136.
(45) Kaltak, M.; Klimeš, J.; Kresse, G. A cubic scaling algorithm for the random phase approximation: Defect calculations for large Si model structures. Submitted for publication.
(46) Mattuck, R. D. *A Guide to Feynman Diagrams in the Many-body Problem*; Dover Books on Physics Series; Dover Publications: New York, 1976
(47) Perdew, J. P.; Ernzerhof, M.; Burke, K. Rationale for mixing exact exchange with density functional approximations. *J. Chem. Phys.* **1996**, *105*, 9982−9985.
(48) Perdew, J. P.; Burke, K.; Ernzerhof, M. Generalized Gradient Approximation Made Simple. *Phys. Rev. Lett.* **1996**, *77*, 3865−3868.